

Complementary Effects of Porosigen and Stabiliser on the Structure of Hollow Porous Poly(lactic-co- glycolic acid) Microparticles

Authors: Xiaoqian Su,[†] Ipshita Gupta,[†] Umesh Sai Jonnalagadda,[†] and James J. Kwan^{‡,}*

[†] School of Chemical and Biomedical Engineering, Nanyang Technological University,
Singapore, 637459

[‡] Department of Engineering Science, University of Oxford, Oxford OX3 7DQ, United
Kingdom.

KEYWORDS: poly(lactic-co-glycolic) acid, porosigens, hollow microparticles, porous
microparticles, drug release kinetics

ABSTRACT

Poly(lactic-co-glycolic acid) (PLGA) plays a pivotal role in both conventional and emerging drug
delivery applications. In this paper, we utilize a facile synthesis strategy to fabricate PLGA
microparticles with shapes including the conventional hollow sphere and exotic shapes such as
multi-cavity particles and cage-like particles. These shapes are obtainable at sizes between 0.6 and
6 micrometers in diameter. Electron microscopy images indicated the presence of water droplets
in the oil phase of the emulsion, suggesting that excess salinity in the aqueous core facilitated water

permeation from the bulk aqueous solution through the organic layer. These aqueous droplets in the oil phase later become the pores and surface cavities on the particles. Using Rhodamine B as a model drug, we measured both loading efficiencies and payload release profiles for all PLGA formulations and indicated a correlation between particle shape and drug release mechanism. Our report elucidates the roles of stabilisers and porosigens on the control of both size and shape of PLGA microparticles, providing a simple framework to produce a wide range of loadable PLGA microparticles with exotic shapes.

INTRODUCTION

Poly(lactic-co-glycolic acid) (PLGA) is a polymer known for its hydrolytic degradation and biocompatibility.¹ Micro- and nanoparticles comprised of PLGA have played a vital role for many current and emerging drug release strategies^{2,3} for the treatment cancer⁴ and vascular⁵ and pulmonary disorders.⁶ Particle composition, size, and structure are all crucial for their pharmacokinetics,⁷ biodistribution,⁸ degradation kinetics,⁹ and drug loading capabilities.¹⁰ One particular structure of PLGA particles of interest are hollow porous particles due to the larger specific surface area with lower density resulting from the pores.⁶ Similarly, nano- and microparticles with surface cavities have also been shown to trap surface bubbles that respond to ultrasound, enabling ultrasound-enhanced drug delivery strategies.^{11–13} These more exotic structures are desirable for many drug delivery applications.^{14,15}

Considering the significance of hollow porous PLGA particles, the procedures for their fabrication and their resulting properties have been extensively studied. To consistently form a hollow structure, a double emulsion technique is often used to nest an aqueous core within an oil or organic layer comprised of the polymeric component.¹⁶ This technique creates a water-oil-water

(W/O/W) mixture that allows facile and efficient introduction of functional components (e.g., therapeutic agents) either within the aqueous particle core or the polymeric shell. The aqueous core may then be removed through freeze drying, resulting in a hollow micro- or nanosphere. To control the size and shape of the PLGA particles, a combination of stabilizers and porosigens are added. Stabilizers such as polyvinyl alcohol (PVA) self-assemble at the water-oil interface, preventing coalescence and Ostwaldt ripening during and after the emulsification process.¹⁷ In contrast, porosigens such as ammonium bicarbonate,⁶ polymers,^{14,18} oils,¹⁹ and salts (e.g., sodium chloride²⁰ and calcium chloride²¹), have been added into the aqueous core as a means to produce pores across the surface of the PLGA shell. As a result, there have been a multitude of formulations presented to address the specific drug delivery challenges of the chosen application.

The use of porosigens often induces swelling of the emulsions, yielding porous yet relatively large ($\geq 5 \mu\text{m}$ in diameter) particles. These sizes are undesirable for many systemic drug delivery applications that benefit from highly porous particles,¹⁴ and as a result have been limited to predominantly pulmonary drug delivery applications.⁶ Though it has been established that the interplay between porosigens and PVA stabilisers influence the size and porosity of the resulting particles, there remains a challenge in producing small ($< 5 \mu\text{m}$ in diameter) porous and hyper-porous particles.

Here, we report on the complementary relationship between phosphate buffered saline (PBS) solution as the porosigen and PVA as the stabilizer on the resulting structure of PLGA microparticles formed by double emulsion methods. We showed that tuning both the PBS concentration in the internal aqueous droplet and the PVA concentration in the bulk aqueous solution produced hollow PLGA microparticles with broad range of shapes (from conventional hollow spheres to more exotic cage-like particles) and sizes (from $0.6 \mu\text{m}$ to $6 \mu\text{m}$ in diameter).

To better understand the role of salts as a porosogen, we investigated the influence of the individual components of PBS (i.e., chloride and phosphate salts) on the structure and size of PLGA microparticles. Interestingly, phosphate salts produced the most porous structures at lower concentrations compared to the chloride salts. We also provide visual evidence of the presence of water droplets in the oil phase of the double emulsion for the first time, validating the hypothesis that salt-based porosogens in the internal aqueous phase create an osmotic gradient across the organic phase, thereby promoting water transport into the oil phase. By using a fluorescent dye as a model drug, we measured both encapsulation efficiencies and release profiles of each formulation produced. Fitting the drug release profiles of our profiles indicated that the shape of the particle correlated with the release mechanism. Our report expands on the capability to control both size and shape of the PLGA microparticles and improves our understanding on the pore formation process to enable the production of smaller multi-cavity and porous hollow PLGA microparticles ideal for both conventional and emerging drug delivery applications.

METHODS

Materials and Reagents

Poly(lactide-co-glycolide 50:50) (PLGA, ResomerRG504 H), Poly(vinyl alcohol) (PVA) (Mw 9,000-10,000, 80% hydrolyzed), Dichloromethane (anhydrous, $\geq 99.8\%$), Rhodamine B (RhB), Phosphate buffered saline (PBS) tablets, sodium chloride, potassium chloride, sodium phosphate dibasic dihydrate, and potassium phosphate monobasic were purchased from Sigma-Aldrich and used as received. Deionized water was obtained from a pure water system (Stakpure, Germany).

Preparation of hollow microparticles

The fabrication method for double emulsion procedures is as follows. 50 mg of PLGA and 0.5 mg of RhB was dissolved in 2 mL of dichloromethane (DCM). Then 100 μ l of PBS was added to the organic mixture and sonicated (Ultrasonic processor VCX 130, Sonics and Materials Inc., USA) at 100 W for 30 s in an ice bath to form an emulsion. The obtained W/O emulsion was poured into a PVA solution and homogenized over ice for 5 min. Then this particle suspension was stirred for 3 h in a chemical fume hood to allow organic solvent evaporation. The PLGA particles were collected by centrifugation at 1,000 G for 5 min, after which they were redispersed and washed three times with distilled water. After the final wash, the microparticles were freeze dried (Alpha 2-4 LSCbasic, Christ, Germany) for 48 h to achieve a dried powder for long term storage. The formulations investigated were 0x, 1x, 5x, and 10x PBS, and 1%, 3%, 5%, and 10% PVA. 1x PBS is given as 0.01 M concentration in accordance to the manufacture instructions.

Characterization of Microparticles

Size and the surface morphology of PLGA microparticles were assessed using a JEOL JSM-6700 field emission scanning electron microscope (FE-SEM; JEOL Ltd, Japan) at an acceleration voltage of 5 kV. Transmission electron microscopy (TEM, JEOL JEM-1400, Japan) was operated at 120 kV. Size distributions were determined by dynamic light scattering (DLS) (Malvern Nano-ZS, UK). Fluorescence images of PLGA microparticles were collected using a confocal laser scanning microscope (LSM 800, Zeiss, Germany).

The quantity of RhB present was calculated according to the UV-absorbance of the dye at 553 nm measured by a UV-Vis Spectrometer (Shimadzu UV 2450, Shimadzu Corporation, Japan). The encapsulation efficiency was calculated by first measuring the remaining RhB within in the supernatant of RhB-mcPLGA microparticles after solvent evaporation and subtracting it from the

total amount of RhB added into the system. This difference was divided by the total amount of RhB added and multiplied by 100 to obtain the percent of RhB encapsulated.

Release of RhB

In vitro release of RhB was performed using a sample and separation method. 25 mg of freeze-dried RhB-mcPLGA microparticles were collected and dispersed in 50 ml of 0.01 M PBS (pH 7.4) buffer solution in sealed vials. This solution was maintained at 37°C with shaking at 300 rpm. At each time point, 1 ml of the solution was taken out and analyzed using a UV-visible spectrophotometer at 553 nm using the methods described earlier. The release profile was determined by the amount of RhB delivered (M_t) to the amounts of effectively encapsulated RhB (M_0), as a function of time. The experiment was performed in triplicate.

RESULTS

Effect of PBS and PVA on the structure of microparticles

SEM images of PLGA microparticles prepared using the double emulsion-diffusion-evaporation method exhibited a multitude of sizes and porosity depending on the proportion of porosigen and stabilizer, as shown in Figure 1. RhB was also encapsulated as indicated by fluorescent images of the PLGA microparticles (Figure 1 insets). In Figure 1, we categorized the particles as either hollow sphere, surface pores, cage-like, or multi-cavity based on the predominant particle found in the images. PLGA microparticle formulations without PBS in the internal aqueous phase lacked pores, irrespective of the quantity of PVA in the external aqueous phase. Furthermore, these particles were all hollow with relatively uniform shell thickness. Increasing the aqueous core PBS concentration to 1x resulted in small and infrequent surface pores for all PLGA particles synthesized, regardless of the quantity of PVA present in the bulk aqueous phase.

For 10x and 20x PBS in the internal aqueous phase, a mixture of surface pores, pore tunnels, and surface cavities became present on the shell of the PLGA particles. These microparticles were not uniformly spherical; cup shapes, multi-cavity surfaces, and miscellaneous cage-like shapes were also present. Large pores across the entire surface of the hollow sphere formed spherical cage-like structures for formulations with low (< 3 wt%) PVA. At higher concentrations of PVA, the pores did not permeate through the entire shell of the PLGA microparticle. Instead cavities on the surface formed, which ranged in size and number. The fluorescent images also recapitulated the features of the PLGA microparticles observed on the SEM, and also indicated that nearly all particles observed were hollow.

Particle size analysis by DLS of the PLGA microparticles (Figure 2) indicated that the addition of salt increased the size of the PLGA microparticles. Conversely, increasing the concentration of PVA in the external aqueous phase reduced the diameter of the PLGA microparticles. For all of the PLGA particles measured by DLS, the polydispersity index (PDI) was below 0.3 (ranging from 0.098 to 0.256), which is below the maximum size distribution accepted for drug delivery applications.²²

Considering the important role that the concentration of PBS in the internal aqueous phase plays on the presence of pores on the surface of the PLGA microparticles, we next investigated the pore-forming process in more detail. Representative TEM images of W/O/W emulsions at different times during the solvent evaporation process are shown in Figure 3a. An illustration detailing this process is provided in Figure 3b. From these images, aqueous droplet formation within the organic phase was evident at all time points, which appeared to grow in size and number as time progressed. Salt precipitation was also evident as dark patches in the organic phase. As the organic solvent

evaporated over time, it was evident from the TEM images that the PLGA solidified and trapped the secondary aqueous droplets, forming the final structure of the particles.

Given that PBS is comprised of four different salts (disodium hydrogen phosphate, sodium chloride, potassium chloride, and potassium dihydrogen phosphate), we next examined if the pore formation was dominated by any single salt in the solution. Representative SEM images of PLGA particles (Figure 4a) manufactured with aqueous cores consistent of the individual salts of 10x PBS indicated that pore formation predominantly formed due to the presence of sodium chloride and disodium phosphate. Few, if any, pores formed on the microparticles using the other salts (potassium chloride and potassium phosphate) in the aqueous core. Considering the large difference in the quantity of the different salts between each component of the PBS, we also manufactured microparticles using equivalent concentrations (0.1 M) of the salt components and no salt as a control. The SEM images (Figure 4b) indicated that 0.1 M of salt within the internal aqueous phase permitted pore formation, irrespective of the salt used. For sodium chloride and potassium chloride, the pores were singular, small, and did not breach through the entire shell. In contrast, the phosphate salts formed a mixture of particles with larger and more numerous pores that permeated through the entire PLGA shell as well as large singular pores that deformed the particles into ‘bowl-like’ shapes. TEM images of W/O/W emulsions at different solvent evaporation times (Figure 5) confirmed the predominant presence of secondary aqueous droplets within the organic phase for particles formulated with phosphate salts. Further increasing the salt concentration to 1 M across all salt types ensured pore formation (Figure S1). Using disodium phosphate, no stable structure was present.

Encapsulation Efficiency and Release Profile of Model drug

The encapsulation efficiency of fabricated PLGA microparticles is summarized in Figure 6. Generally, an increase in the external aqueous concentration of PVA resulted in a decrease in loading efficiency. Interestingly, the concentration of salt in the internal aqueous phase did not affect the loading efficiency.

Next, we measured the release of RhB from the PLGA microparticles comparing the effect of concentrations of PBS and PVA in the particle formulations on the rates of RhB release (Figure S2). The release of RhB for all formulations tested followed a rapid rate of release within the first 24 hours, after which there was a stagnation of release. Without any PBS present in the formulation, the release rate of RhB generally increased with increasing concentration of PVA. However, this effect became less pronounced for formulations with higher concentrations of PBS in the internal aqueous core. That being said, the total amount of RhB released at 72 hours was noticeably lower for formulations using 20x PBS irrespective of the quantity of PVA. Similarly, increasing the concentration of PBS at 1% PVA also generally improved the rates of RhB release, and this too was less evident as the concentration of PVA was increased to 10%.

Release of RhB from all of the PLGA microparticles fitted a Korsmeyer-Peppas model (Equation 1).²³

$$M_t/M_\infty = kt^n \quad (\text{Eq. 1})$$

where M_t is the concentration of RhB released at a given point in time, M_∞ is the equilibrium concentration of RhB in the solution, k is the release rate of RhB, t is time, and n is the time constant. Table 1 summarizes the fitting parameters of the Korsmeyer-Peppas model (for values of M_t/M_∞ approximately less than 0.6) of all the PLGA formulations. Increasing PBS at fixed PVA concentrations increased RhB release rates of the resulting microparticles (Figure S3a). For particles formulated with 0x and 1x PBS, increasing PVA (decreasing size) resulted in a monotonic

increase in release rate (Figure S3b). In contrast, particles formulated with PBS concentrations at an above 10x had release rates that initially increased before decreasing with increasing PVA concentrations. By plotting the release rates of the different formulations as a function of particle size (Figure 7), it became evident that the release rates were correlated to both size and shape of the particle. Generally, hollow sphere and surface pore particles had slower release kinetics compared to both multi-cavity and cage-like particles.

DISCUSSION

PLGA microparticles are one of the most widely studied drug delivery systems with usage across a broad range of applications.² As a result, there is a continued interest in the formulation and manufacturing procedures to improve loading capacity,²⁴ circulation time,⁸ and functional capability.²⁵ Both size and shape of these particles play a role in their capacity to function as drug delivery vehicles. Hollow PLGA microparticles are of particular interest owing to their ability to encapsulate water soluble drugs such as small molecular therapeutics²⁶ and proteins.²⁷ Surface architecture of the PLGA microparticles have also been shown to play an important role. Porous and multi-cavity structures, for example, have larger surface area to volume ratios compared to smooth spheres, resulting in faster degradation,⁹ lower mass median aerodynamic diameter (MMAD),⁶ and are able to trap gas to provide ultrasound-responsiveness.²⁸ With such a broad range of applications, PLGA microparticle formulations are typically tailored to the specific application with occasional unifying features between different formulations.

At present, the production of these particles is governed by the manufacturing technique, polymer formulation, and selected adjuvants (porosigens, drug, etc.).²⁹ For example, the well-established double emulsion method is capable of producing large and small hollow microspheres

through the use of emulsion stabilisers. Similarly, this method has also enabled the production of large multi-cavity and porous hollow microparticles for use as inhalation agents^{6,14} by the addition of various porosigens. Surprisingly, the production of smaller and sub-micron porous or multi-cavity particles have not yet been achieved, despite their potential as systemic drug delivery agents and ultrasound contrast agents.

Here, we have successfully manufactured both multi-cavity and porous microparticles with particle diameters as small as 0.6 μm , nearly an order of magnitude smaller than previous efforts. Here, salts were used as a porosigen to produce cavities and pores on the hollow particles. Though it is well-known that salts induce pore formation on hollow spheres,²⁰ salts also induce a substantial amount of swelling,^{30,31} resulting in particle diameters not suitable for systemic drug delivery. The swelling of the emulsions to form large particles was also evident in our SEM images and DLS diameter measurements. To mitigate this swelling, PVA was added into the bulk aqueous phase as a stabilizer.³¹

As expected, we observed that the PVA reduced the size of the particle regardless of the salt concentration in the internal aqueous phase. This reduction in size occurred because PVA prevented the coalescence of the W1/O droplets, thereby maintaining the stability of the W1/O/W2 emulsion during the formation of the PLGA microparticles.³² Previous studies reported a significant reduction in particle size by increasing PVA concentration in the external water phase when PVA concentration is smaller than 5%.^{32, 33} Our observations were in agreement with previous results suggested that the presence of PVA in the external water phase stabilizes emulsion droplets against coalescence, resulting in smaller emulsion droplets.³⁴ Above 5% w/v of PVA, only a small quantity of stabilizer will be adsorbed at the interface; excess PVA will remain in the continuous aqueous phase and does not further contribute to the stabilization of the W/O droplet.³⁵

As mentioned earlier, the presence of salts in the internal aqueous phase results in the formation of surface pores and tunnels. Salts such as PBS behave as a porosigen because it provides an Osmotic pressure gradient, forcing water from the bulk phase to diffuse into the organic phase. As water enters into the organic phase, it phase-separates to form secondary droplets throughout the organic phase. Though earlier work^{20,21} did not directly observe this process, we were able to observe aqueous droplets throughout the organic phase only within particles formulated with PBS in our TEM images. Although this study primarily utilized PBS to induce pore formation, investigation of the individual components of PBS confirmed that each salt component was capable of forming pores. Considering the importance of Osmotic pressure in the aqueous core, that the molar concentration of ions in the internal aqueous phase and the van 't Hoff index (i) of the salt were critical to pore formation. For example, 0.1 M of the chloride salts ($i = 2$) yielded small single pores on the surface of the particle. In contrast, the same molar quantity of disodium phosphate ($i = 3$) yielded larger cage-like structures. Interestingly, the potassium phosphate salt ($i = 2$) also produced both cage-like and multi-cavity particles, suggesting that the phosphate ions may have further enhanced pore formation in comparison to the chloride ions. In fact, when large quantities of disodium phosphate were added to the internal aqueous phase, stable particles were unable to form, potentially due to the excess of water in the organic phase destabilizing the emulsion. Therefore, the formation of the pores on the surface of the hollow microparticles stemmed from the interplay between the salt concentration in the internal aqueous phase and the concentration of stabilizer in the external aqueous phase. Increasing the stabilizer concentration also modified the final structure of the particle, transitioning the large hollow cage-like structures to smaller particles with single to multiple surface cavities.

Salt porosigens are also linked to reduced encapsulation efficiencies,³⁶ limiting their efficacy as drug delivery vehicles. In our work, PBS had no substantial effect on the encapsulation efficiencies. The encapsulation efficiency did however decrease with increasing amounts of PVA. One reason for this observation may be due to the decrease in particle diameter as a result of increased amounts of PVA in the formulation.³⁷ Furthermore the model drug, RhB, used here was slightly amphiphilic. Thus, at higher concentrations of PVA in the external aqueous phase, RhB may diffuse out of the organic phase and solubilize into the core of PVA micelles in the aqueous phase.^{38,39} This leaching effect and PVA micelle enhanced solubility of RhB in the aqueous phase may have resulted in a further reduction in the encapsulation efficiency of our particles.

We observed a rapid release of our model drug, RhB in the first 24 hours for all formulations. It is known that drug release from biodegradable microparticles is controlled by diffusion and erosion.^{40,41} Initially, the release phase is controlled by the diffusion through the polymeric matrix and water-filled pores, according to the drug transport properties. The second process involves bulk erosion: the polymer matrix uptakes water and the polymer chains are degraded and made small enough to be soluble, and drug is released during the dissolution of the PLGA matrix, which will in turn accelerate the diffusion rate of the releasing drug.⁴² For porous particles, transport through aqueous pores is the principal transport mechanism.⁴³ For small molecule drugs that will diffuse through the matrix much faster it may be expected that the exhaustion of the release device will occur before the total degradation and erosion of the polymer matrix.⁴⁴

The release data from PLGA microparticles fit well to the Korsmeyer-Peppas equation. The Korsmeyer-Peppas equation comprises of two key fitting variables, 'k' the release constant and 'n' the exponent constant. We observed that the k-values for non-porous and porous spherical PLGA particles increased as the size of the particles decreased. This observation was consistent with

previous studies¹⁰, which reported that drug release was inversely proportional to the size of the microspheres due to decreased diffusional path length and increased effective surface area of the microspheres. Interestingly, the release rates increased as the particles became more porous and larger in size. This unexpected increase in release rates may be governed by the increased surface area presented by the pores. With increasing particle diameter, the number and size of surface cavities or tunnels also increases. The exponent constant 'n' may provide further insight into the unexpected increase in release constant for the more exotic shapes.

The diffusional exponent 'n' specifies the mechanism of drug release. From our model fit, spherical and porous particles had a n-values greater than 0.43. Values above 0.43 are typically indicative of anomalous drug transport, which may suggest that drug release from the spherical and porous particles was due to both Fickian diffusion of drug from the PLGA polymer matrix as well as release from the hydrolytic degradation and subsequent erosion of the PLGA polymer matrix. In stark contrast, the release constant for cage-like and most of the multi-cavity particles was below 0.43. This suggested that the drug release mechanism was governed predominantly by Fickian diffusion.⁴⁵ We hypothesize that the thin walls of the cavities and the presence of tunnels that formed the cage-like particles enabled a substantial increase in surface area that promoted Fickian diffusion. Our results suggested that multi-cavity and cage-like particles may deliver their payload faster than the complete degradation of the PLGA polymer matrix. Therefore, it may become crucial to consider not only the polymer formulation, but also the particle size and shape as part of the design of the particle for the specific drug delivery application.

CONCLUSION

307 Here we report on the facile fabrication of PLGA hollow structures with PBS as the porosigen
308 and PVA as the stabilizer. We showed that tuning both the salt concentration in the internal
309 aqueous droplet and the PVA concentration in the bulk aqueous solution, produced hollow PLGA
310 microparticles with broad range of shapes (from conventional hollow spheres to more exotic cage-
311 like particles) and sizes (from 6 μm to as small as 0.6 μm in diameter). Increasing the concentration
312 of PVA in the external aqueous phase reduced the diameter of the PLGA microparticles.
313 Conversely, the addition of PBS in the internal phase increased the size and porosity of the PLGA
314 microparticles owing to the Osmotic driving force for the transport of water from the bulk aqueous
315 phase to the internal aqueous phase, which was visually observed with TEM for the first time.
316 Among the four different salts of PBS, phosphate salts produced a highly porous structure
317 compared to the chloride salts. The release of drug from spherical and porous microparticles was
318 governed by anomalous transport. In contrast, release of RhB from multi-cavity and cage-like
319 microparticles was primarily governed by Fickian diffusion. This study provides a framework for
320 the facile production and design consideration for conventionally and exotically shaped
321 microspheres ideal for emerging drug delivery applications.

322 ASSOCIATED CONTENT

323 **Supporting Information.** Supporting Information is available from the author.

324 AUTHOR INFORMATION

325 **Corresponding Author**

326 * james.kwan@eng.ox.ac.uk

327 **Author Contributions**

328 The manuscript was written through contributions of all authors. All authors have given approval
329 to the final version of the manuscript. The authors have no conflicts of interest.

330 ACKNOWLEDGMENT

331 This research is supported by the Singapore Ministry of Health's National Medical Research
332 Council under its NMRC/OFYIRG/0034/2017.

333

334 REFERENCES

- 335 (1) Kapoor, D. N.; Bhatia, A.; Kaur, R.; Sharma, R.; Kaur, G.; Dhawan, S. PLGA: A Unique
 336 Polymer for Drug Delivery. *Ther. Deliv.* **2015**, *6* (1), 41–58.
 337 <https://doi.org/10.4155/tde.14.91>.

- 338 (2) Makadia, H. K.; Siegel, S. J. Poly Lactic-Co-Glycolic Acid (PLGA) as Biodegradable
 339 Controlled Drug Delivery Carrier. *Polymers (Basel)*. **2011**, *3* (3), 1377–1397.
 340 <https://doi.org/10.3390/polym3031377>.

- 341 (3) Danhier, F.; Ansorena, E.; Silva, J. M.; Coco, R.; Le Breton, A.; Préat, V. PLGA-Based
 342 Nanoparticles: An Overview of Biomedical Applications. *J. Control. Release* **2012**, *161* (2),
 343 505–522. <https://doi.org/10.1016/j.jconrel.2012.01.043>.

- 344 (4) Yallapu, M. M.; Gupta, B. K.; Jaggi, M.; Chauhan, S. C. Fabrication of Curcumin
 345 Encapsulated PLGA Nanoparticles for Improved Therapeutic Effects in Metastatic Cancer
 346 Cells. *J. Colloid Interface Sci.* **2010**, *351* (1), 19–29.
 347 <https://doi.org/10.1016/j.jcis.2010.05.022>.

- 348 (5) Chung, H. J.; Kim, H. K.; Yoon, J. J.; Park, T. G. Heparin Immobilized Porous PLGA
 349 Microspheres for Angiogenic Growth Factor Delivery. *Pharm. Res.* **2006**, *23* (8), 1835–
 350 1841. <https://doi.org/10.1007/s11095-006-9039-9>.

- 351 (6) Yang, Y.; Bajaj, N.; Xu, P.; Ohn, K.; Tsifansky, M. D.; Yeo, Y. Development of Highly
 352 Porous Large PLGA Microparticles for Pulmonary Drug Delivery. *Biomaterials* **2009**, *30*
 353 (10), 1947–1953. <https://doi.org/10.1016/j.biomaterials.2008.12.044>.

- 354 (7) Italia, J. L.; Bhatt, D. K.; Bhardwaj, V.; Tikoo, K.; Kumar, M. N. V. R. PLGA Nanoparticles

for Oral Delivery of Cyclosporine: Nephrotoxicity and Pharmacokinetic Studies in Comparison to Sandimmune Neoral®. *J. Control. Release* **2007**, *119* (2), 197–206. <https://doi.org/10.1016/j.jconrel.2007.02.004>.

(8) Avgoustakis, K. Effect of Copolymer Composition on the Physicochemical Characteristics, in Vitro Stability, and Biodistribution of PLGA–MPEG Nanoparticles. *Int. J. Pharm.* **2003**, *259* (1–2), 115–127. [https://doi.org/10.1016/S0378-5173\(03\)00224-2](https://doi.org/10.1016/S0378-5173(03)00224-2).

(9) Klose, D.; Siepmann, F.; Elkharraz, K.; Krenzlin, S.; Siepmann, J. How Porosity and Size Affect the Drug Release Mechanisms from PLGA-Based Microparticles. *Int. J. Pharm.* **2006**, *314* (2), 198–206. <https://doi.org/10.1016/j.ijpharm.2005.07.031>.

(10) Acharya, G.; Shin, C. S.; Vedantham, K.; McDermott, M.; Rish, T.; Hansen, K.; Fu, Y.; Park, K. A Study of Drug Release from Homogeneous PLGA Microstructures. *J. Control. Release* **2010**, *146* (2), 201–206. <https://doi.org/10.1016/j.jconrel.2010.03.024>.

(11) Kwan, J. J.; Myers, R.; Coviello, C. M.; Graham, S. M.; Shah, A. R.; Stride, E.; Carlisle, R. C.; Coussios, C. C. Ultrasound-Propelled Nanocups for Drug Delivery. *Small* **2015**, *11* (39), 5305–5314. <https://doi.org/10.1002/smll.201501322>.

(12) Su, X.; Thomas, R. G.; Bharatula, L. D.; Kwan, J. J. Remote Targeted Implantation of Sound-Sensitive Biodegradable Multi-Cavity Microparticles with Focused Ultrasound. *Sci. Rep.* **2019**, *9* (1), 1–13. <https://doi.org/10.1038/s41598-019-46022-0>.

(13) Thomas, R. G.; Jonnalagadda, U. S.; Kwan, J. J. Biomedical Applications for Gas-Stabilizing Solid Cavitation Agents. *Langmuir* **2019**, *35* (31), 10106–10115. <https://doi.org/10.1021/acs.langmuir.9b00795>.

- 376 (14) Ni, R.; Muenster, U.; Zhao, J.; Zhang, L.; Becker-Pelster, E.-M.; Rosenbruch, M.; Mao, S.
377 Exploring Polyvinylpyrrolidone in the Engineering of Large Porous PLGA Microparticles
378 via Single Emulsion Method with Tunable Sustained Release in the Lung: In Vitro and in
379 Vivo Characterization. *J. Control. Release* **2017**, *249*, 11–22.
380 <https://doi.org/10.1016/j.jconrel.2017.01.023>.
- 381 (15) Kim, H. K.; Chung, H. J.; Park, T. G. Biodegradable Polymeric Microspheres with
382 “Open/Closed” Pores for Sustained Release of Human Growth Hormone. *J. Control.*
383 *Release* **2006**, *112* (2), 167–174. <https://doi.org/10.1016/j.jconrel.2006.02.004>.
- 384 (16) Lee, D.; Weitz, D. A. Double Emulsion-Templated Nanoparticle Colloidosomes with
385 Selective Permeability. *Adv. Mater.* **2008**, *20* (18), 3498–3503.
386 <https://doi.org/10.1002/adma.200800918>.
- 387 (17) Kwon, H.-Y.; Lee, J.-Y.; Choi, S.-W.; Jang, Y.; Kim, J.-H. Preparation of PLGA
388 Nanoparticles Containing Estrogen by Emulsification–Diffusion Method. *Colloids Surfaces*
389 *A Physicochem. Eng. Asp.* **2001**, *182* (1–3), 123–130. [https://doi.org/10.1016/S0927-](https://doi.org/10.1016/S0927-7757(00)00825-6)
390 [7757\(00\)00825-6](https://doi.org/10.1016/S0927-7757(00)00825-6).
- 391 (18) M, O.; Kim, S. C.; Shim, Y. K.; Lee, W. K. Preparation of “Open/Closed” Pores of PLGA-
392 Microsphere for Controlled Release of Protein Drug. *Mong. J. Chem.* **2018**, *18* (44), 41–47.
393 <https://doi.org/10.5564/mjc.v18i44.936>.
- 394 (19) Arnold, M. M.; Gorman, E. M.; Schieber, L. J.; Munson, E. J.; Berkland, C. NanoCipro
395 Encapsulation in Monodisperse Large Porous PLGA Microparticles. *J. Control. Release*
396 **2007**, *121* (1–2), 100–109. <https://doi.org/10.1016/j.jconrel.2007.05.039>.

- 397 (20) K. F. Pistel, T. K. Effects of Salt Addition on the Microencapsulation of Proteins Using
398 W/O/W Double Emulsion Technique. *J. Microencapsul.* **2000**, *17* (4), 467–483.
399 <https://doi.org/10.1080/026520400405723>.
- 400 (21) Takai, C.; Hotta, T.; Shiozaki, S.; Matsumoto, S.; Fukui, T. Effect of Inorganic Salt on
401 Formation of Porous PLGA Microspheres. *Chem. Lett.* **2011**, *40* (6), 638–639.
402 <https://doi.org/10.1246/cl.2011.638>.
- 403 (22) Danaei, M.; Dehghankhold, M.; Ataei, S.; Hasanzadeh Davarani, F.; Javanmard, R.;
404 Dokhani, A.; Khorasani, S.; Mozafari, M. Impact of Particle Size and Polydispersity Index
405 on the Clinical Applications of Lipidic Nanocarrier Systems. *Pharmaceutics* **2018**, *10* (2),
406 57. <https://doi.org/10.3390/pharmaceutics10020057>.
- 407 (23) Dash, S.; Murthy, P. N.; Nath, L.; Chowdhury, P. Kinetic Modeling on Drug Release from
408 Controlled Drug Delivery Systems. *Acta Pol. Pharm.* **2010**, *67* (3), 217–223.
409 <https://doi.org/ISSN 0001-6837>.
- 410 (24) Wilkosz, N.; Łazarski, G.; Kovacik, L.; Gargas, P.; Nowakowska, M.; Jamróz, D.;
411 Kepczynski, M. Molecular Insight into Drug-Loading Capacity of PEG–PLGA
412 Nanoparticles for Itraconazole. *J. Phys. Chem. B* **2018**, *122* (28), 7080–7090.
413 <https://doi.org/10.1021/acs.jpcb.8b03742>.
- 414 (25) Zhou, J.; Patel, T. R.; Fu, M.; Bertram, J. P.; Saltzman, W. M. Octa-Functional PLGA
415 Nanoparticles for Targeted and Efficient SiRNA Delivery to Tumors. *Biomaterials* **2012**,
416 *33* (2), 583–591. <https://doi.org/10.1016/j.biomaterials.2011.09.061>.
- 417 (26) Cohen-Sela, E.; Chorny, M.; Koroukhov, N.; Danenberg, H. D.; Golomb, G. A New Double

418 Emulsion Solvent Diffusion Technique for Encapsulating Hydrophilic Molecules in PLGA
 419 Nanoparticles. *J. Control. Release* **2009**, *133* (2), 90–95.
 420 <https://doi.org/10.1016/j.jconrel.2008.09.073>.

421 (27) Ansary, R.; Rahman, M.; Mohamad, N.; Arrif, T.; Latif, A.; Katas, H.; Nik, W.; Awang, M.
 422 Controlled Release of Lysozyme from Double-Walled Poly(Lactide-Co-Glycolide)
 423 (PLGA) Microspheres. *Polymers (Basel)*. **2017**, *9* (12), 485.
 424 <https://doi.org/10.3390/polym9100485>.

425 (28) Straub, J. A.; Chickering, D. E.; Church, C. C.; Shah, B.; Hanlon, T.; Bernstein, H. Porous
 426 PLGA Microparticles: AI-700, an Intravenously Administered Ultrasound Contrast Agent
 427 for Use in Echocardiography. *J. Control. Release* **2005**, *108* (1), 21–32.
 428 <https://doi.org/10.1016/j.jconrel.2005.07.020>.

429 (29) Astete, C. E.; Sabliov, C. M. Synthesis and Characterization of PLGA Nanoparticles. *J.*
 430 *Biomater. Sci. Polym. Ed.* **2006**, *17* (3), 247–289.
 431 <https://doi.org/10.1163/156856206775997322>.

432 (30) Nair, M.; Lusignan, C. P.; Boris, D. C. Colloids and Surfaces A : Physicochemical and
 433 Engineering Aspects Preparation of Uniform Micrometer-Sized Polymer Particles with
 434 Closed-Cell Porous Architecture Made by Limited Coalescence of a Double Emulsion.
 435 *Colloids Surfaces A Physicochem. Eng. Asp.* **2014**, *443*, 583–595.
 436 <https://doi.org/10.1016/j.colsurfa.2013.11.037>.

437 (31) Jiao, J.; Rhodes, D. G.; Burgess, D. J. Multiple Emulsion Stability: Pressure Balance and
 438 Interfacial Film Strength. *J. Colloid Interface Sci.* **2002**, *250* (2), 444–450.
 439 <https://doi.org/10.1006/jcis.2002.8365>.

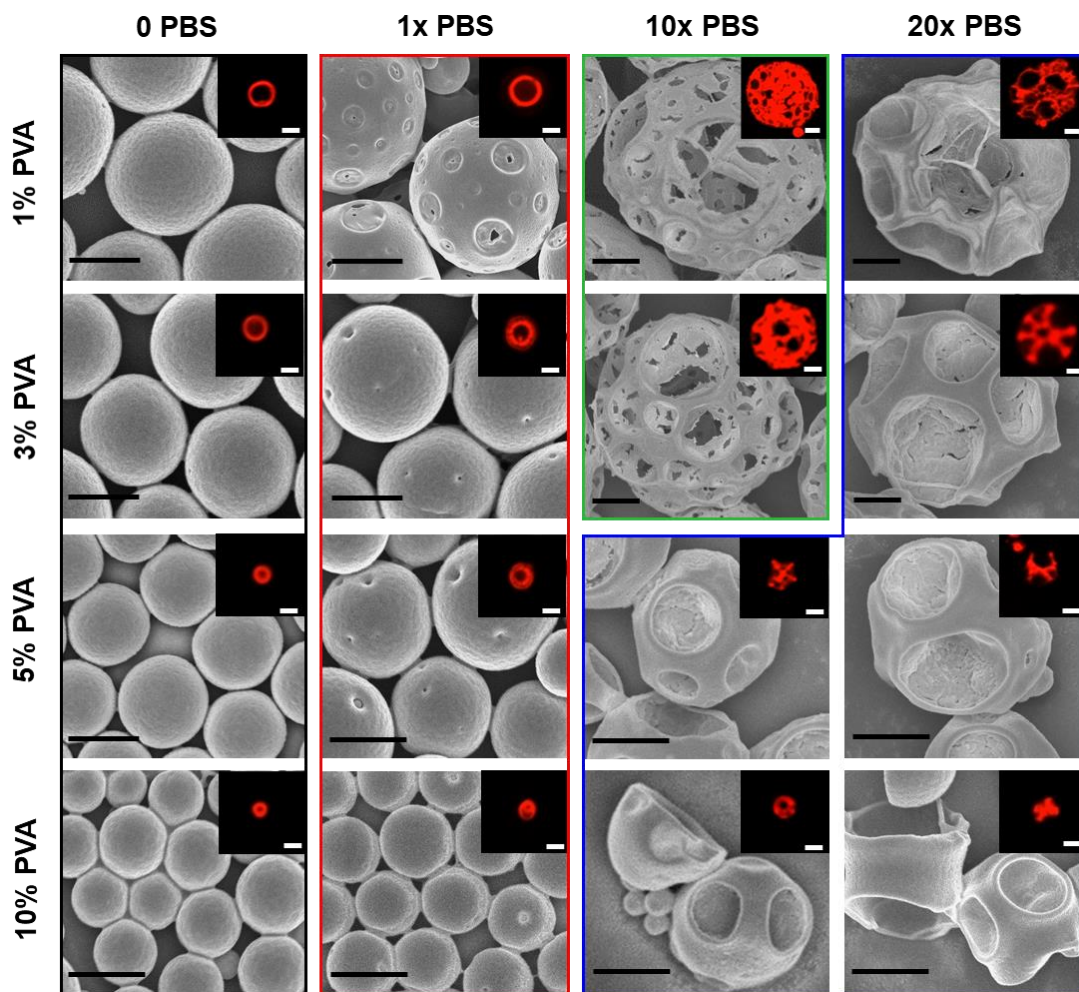
- (32) Quintanar-Guerrero, D.; Fessi, H.; Allémann, E.; Doelker, E. Influence of Stabilizing Agents and Preparative Variables on the Formation of Poly(D,L-Lactic Acid) Nanoparticles by an Emulsification-Diffusion Technique. *Int. J. Pharm.* **1996**, *143* (2), 133–141. [https://doi.org/10.1016/S0378-5173\(96\)04697-2](https://doi.org/10.1016/S0378-5173(96)04697-2).
- (33) Yang, Y. Morphology, Drug Distribution, and in Vitro Release Profiles of Biodegradable Polymeric Microspheres Containing Protein Fabricated by Double-Emulsion Solvent Extraction/Evaporation Method. *Biomaterials* **2001**, *22* (3), 231–241. [https://doi.org/10.1016/S0142-9612\(00\)00178-2](https://doi.org/10.1016/S0142-9612(00)00178-2).
- (34) Sharipova, A.; Aidarova, S.; Mutaliyeva, B.; Babayev, A.; Issakhov, M.; Issayeva, A.; Madybekova, G.; Grigoriev, D.; Miller, R. The Use of Polymer and Surfactants for the Microencapsulation and Emulsion Stabilization. *Colloids and Interfaces* **2017**, *1* (1), 3. <https://doi.org/10.3390/colloids1010003>.
- (35) Jalil, R.; Nixon, J. R. Microencapsulation Using Poly (L-Lactic Acid) II: Preparative Variables Affecting Microcapsule Properties. *J. Microencapsul.* **1990**, *7* (1), 25–39. <https://doi.org/10.3109/02652049009028421>.
- (36) Morlock, M.; Kissel, T.; Li, Y. X.; Koll, H.; Winter, G. Erythropoietin Loaded Microspheres Prepared from Biodegradable LPLG-PEO-LPLG Triblock Copolymers: Protein Stabilization and in-Vitro Release Properties. *J. Control. Release* **1998**, *56* (1–3), 105–115. [https://doi.org/10.1016/S0168-3659\(98\)00070-4](https://doi.org/10.1016/S0168-3659(98)00070-4).
- (37) Choi, H. S.; Seo, S. A.; Khang, G.; Rhee, J. M.; Lee, H. B. Preparation and Characterization of Fentanyl-Loaded PLGA Microspheres: In Vitro Release Profiles. *Int. J. Pharm.* **2002**, *234* (1–2), 195–203. [https://doi.org/10.1016/S0378-5173\(01\)00968-1](https://doi.org/10.1016/S0378-5173(01)00968-1).

- 462 (38) Sharma, N.; Madan, P.; Lin, S. Effect of Process and Formulation Variables on the
463 Preparation of Parenteral Paclitaxel-Loaded Biodegradable Polymeric Nanoparticles: A Co-
464 Surfactant Study. *Asian J. Pharm. Sci.* **2016**, *11* (3), 404–416.
465 <https://doi.org/10.1016/j.ajps.2015.09.004>.
- 466 (39) Song, X.; Zhao, Y.; Hou, S.; Xu, F.; Zhao, R.; He, J.; Cai, Z.; Li, Y.; Chen, Q. Dual Agents
467 Loaded PLGA Nanoparticles: Systematic Study of Particle Size and Drug Entrapment
468 Efficiency. *Eur. J. Pharm. Biopharm.* **2008**, *69* (2), 445–453.
469 <https://doi.org/10.1016/j.ejpb.2008.01.013>.
- 470 (40) Raman, C.; Berkland, C.; Kim, K. (Kevin); Pack, D. W. Modeling Small-Molecule Release
471 from PLG Microspheres: Effects of Polymer Degradation and Nonuniform Drug
472 Distribution. *J. Control. Release* **2005**, *103* (1), 149–158.
473 <https://doi.org/10.1016/j.jconrel.2004.11.012>.
- 474 (41) Tanetsugu, Y.; Tagami, T.; Terukina, T.; Ogawa, T.; Ohta, M.; Ozeki, T. Development of
475 a Sustainable Release System for a Ranibizumab Biosimilar Using Poly(Lactic-Co-Glycolic
476 Acid) Biodegradable Polymer-Based Microparticles as a Platform. *Biol. Pharm. Bull.* **2017**,
477 *40* (2), 145–150. <https://doi.org/10.1248/bpb.b16-00437>.
- 478 (42) Kamaly, N.; Yameen, B.; Wu, J.; Farokhzad, O. C. Degradable Controlled-Release
479 Polymers and Polymeric Nanoparticles: Mechanisms of Controlling Drug Release. *Chem.*
480 *Rev.* **2016**, *116* (4), 2602–2663. <https://doi.org/10.1021/acs.chemrev.5b00346>.
- 481 (43) Fredenberg, S.; Wahlgren, M.; Reslow, M.; Axelsson, A. The Mechanisms of Drug Release
482 in Poly(Lactic-Co-Glycolic Acid)-Based Drug Delivery Systems - A Review. *Int. J. Pharm.*
483 **2011**, *415* (1–2), 34–52. <https://doi.org/10.1016/j.ijpharm.2011.05.049>.

- 484 (44) Hines, D. J.; Kaplan, D. L. Poly(Lactic-Co-Glycolic) Acid-Controlled-Release Systems:
485 Experimental and Modeling Insights. *Crit. Rev. Ther. Drug Carrier Syst.* **2013**, *30* (3), 257–
486 276. <https://doi.org/10.1615/critrevtherdrugcarriersyst.2013006475>.
- 487 (45) Ritger, P. L.; Peppas, N. A. A Simple Equation for Description of Solute Release I. Fickian
488 and Non-Fickian Release from Non-Swellable Devices in the Form of Slabs, Spheres,
489 Cylinders or Discs. *J. Control. Release* **1987**, *5* (1), 23–36. [https://doi.org/10.1016/0168-](https://doi.org/10.1016/0168-3659(87)90034-4)
490 [3659\(87\)90034-4](https://doi.org/10.1016/0168-3659(87)90034-4).
- 491
- 492

493 FIGURES

494



495

496 **Figure 1.** SEM images of PLGA microparticles under different concentrations of PBS and PVA.

497 The insets are the corresponding fluorescence images. The scale bars represent 1 μ m in all images.

498 The predominant shapes of the particles based on the SEM images were categorized as follows:

499 black outlined images represent hollow spheres, red outlined images represent surface pores, green

500 outlined images represent cage-like particles, and blue images represent multi-cavity particles.

501

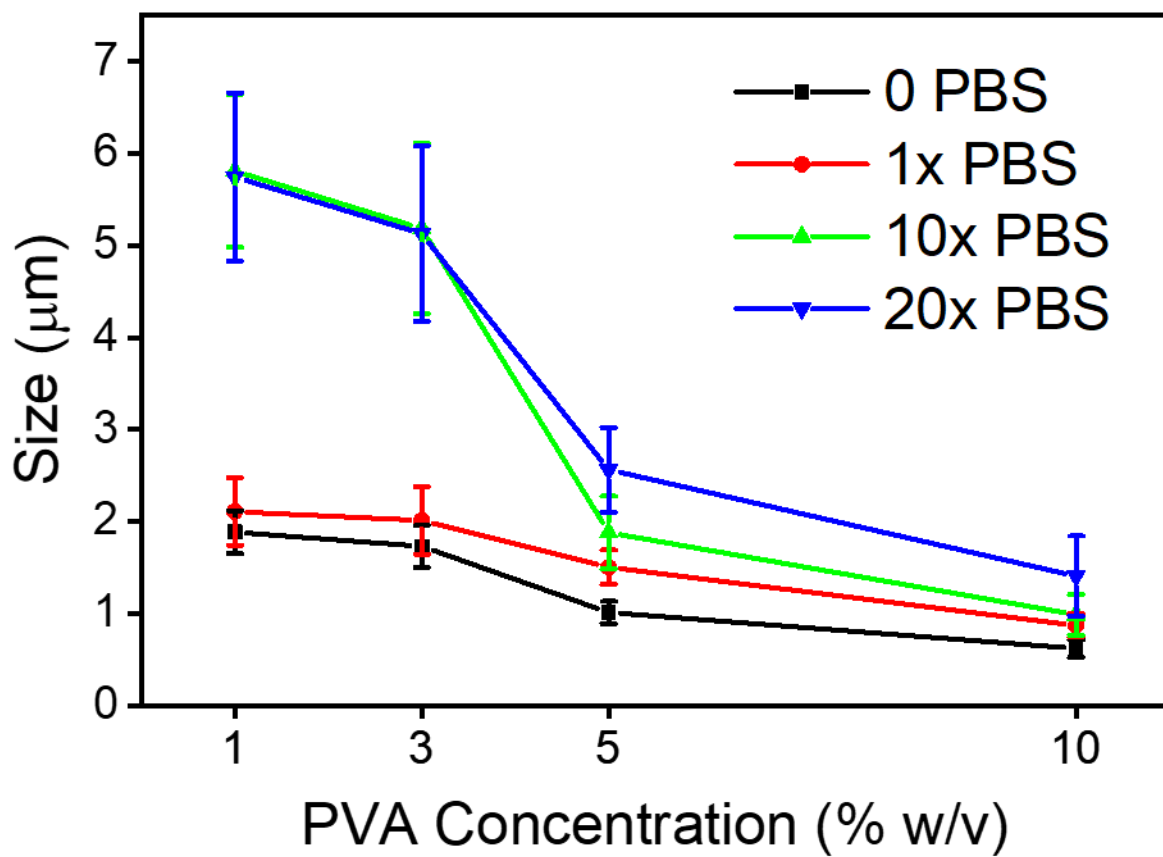


Figure 2. Diameter of PLGA microparticles formulated with different concentrations of PBS and PVA. Data represented as mean \pm SD.

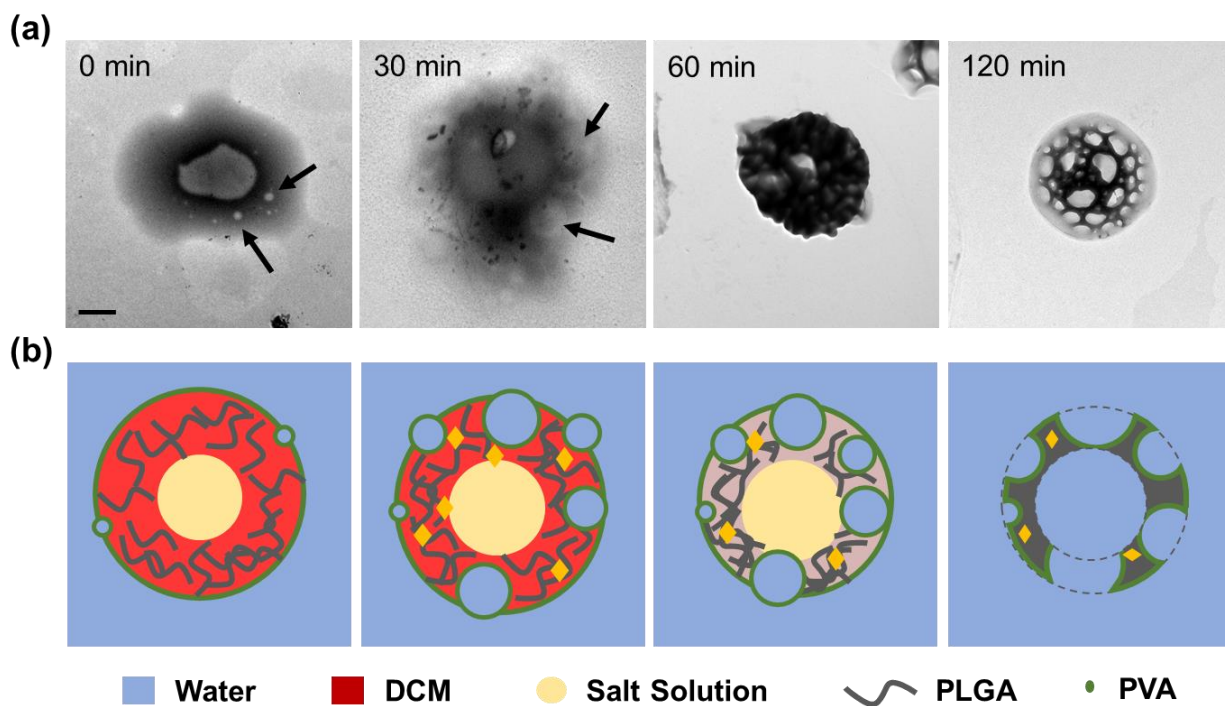


Figure 3. Proposed mechanism for pore formation. (a) TEM images of a W/O/W emulsion at various time points during the evaporation of the organic phase. The scale bars represent 1 μm . (b) A schematic illustration detailing the process.

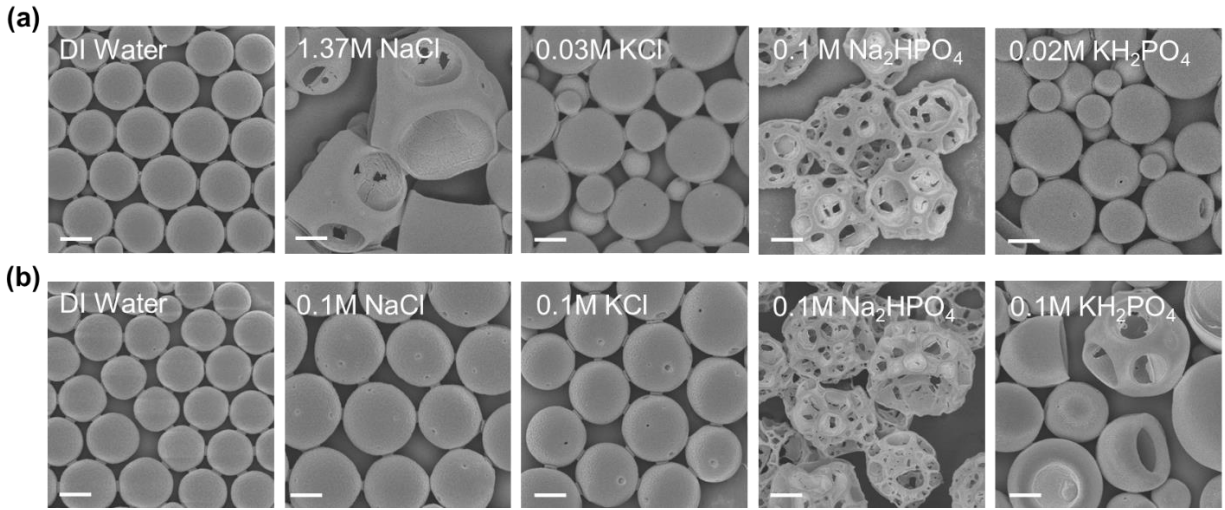


Figure 4. SEM images of PLGA microparticles manufactured with different salts and concentrations. The scale bars represent 1 μm. (a) PLGA particles manufactured with aqueous cores consistent of the individual salts of 10x PBS indicating that pore formation predominantly formed due to the presence of sodium chloride and disodium phosphate. (b) PLGA particles manufactured using 0.1 M of the salt components and no salt as a control indicating that at 0.1M of salt within the internal aqueous phase, irrespective of the type of salt, pore formation occurs.

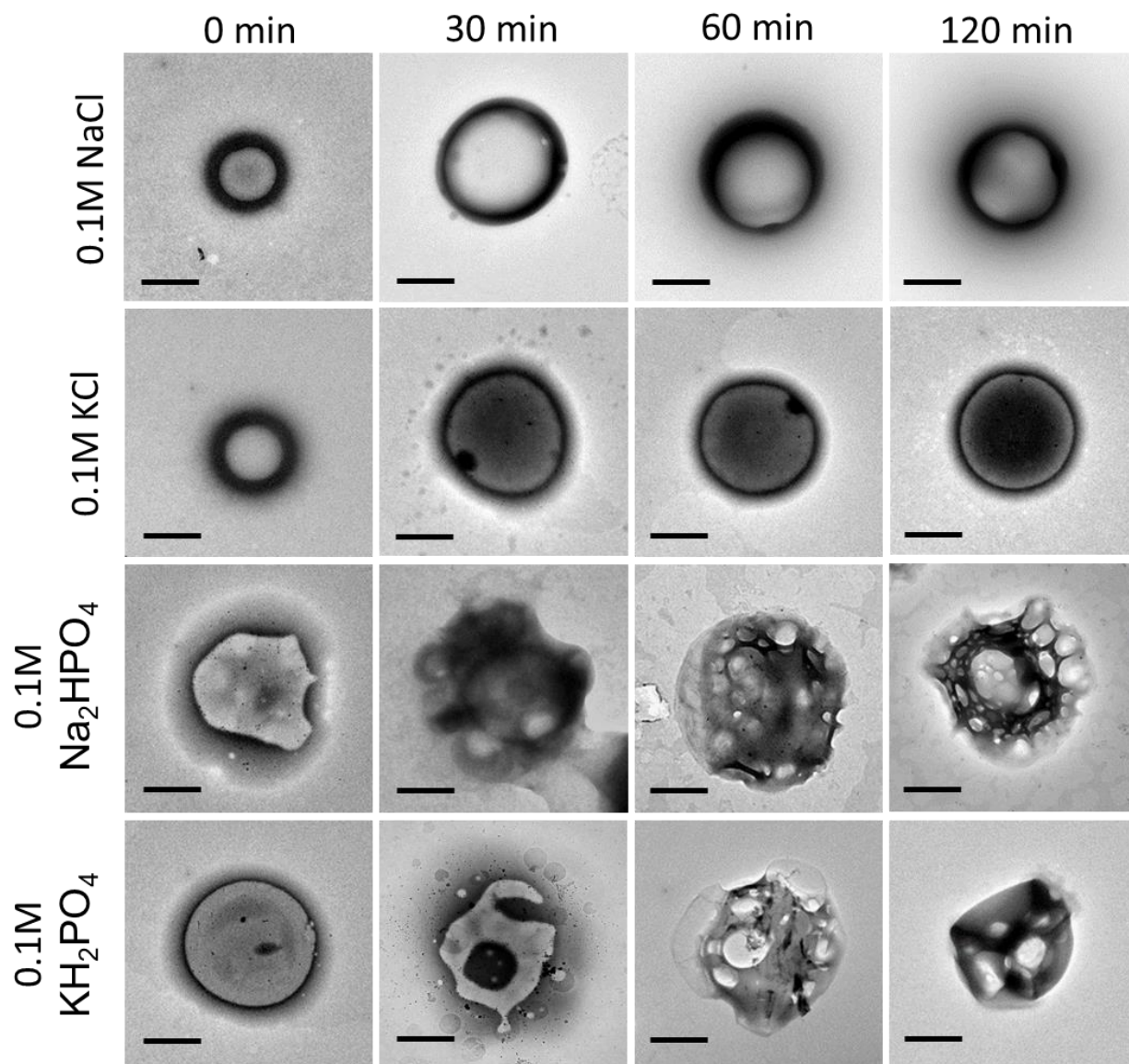
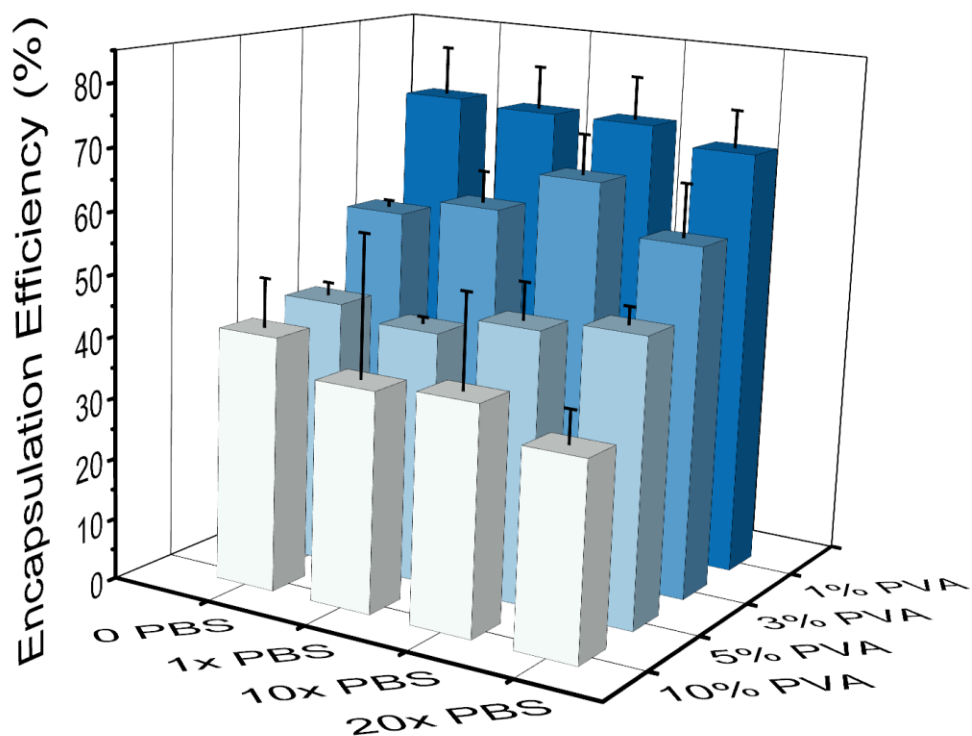


Figure 5. TEM images of W/O/W emulsions at different solvent evaporation times confirmed the predominant presence of secondary aqueous droplets within the organic phase for particles formulated with phosphate salts. The scale bars represent 1 μm .

524



525

526 **Figure 6.** Effect of PBS (0x, 1x, 5x, and 10x) and PVA (1%, 3%, 5%, and 10%) concentration on
527 encapsulation efficiency of PLGA microparticles. Data represented as mean \pm SD (n=3).

528

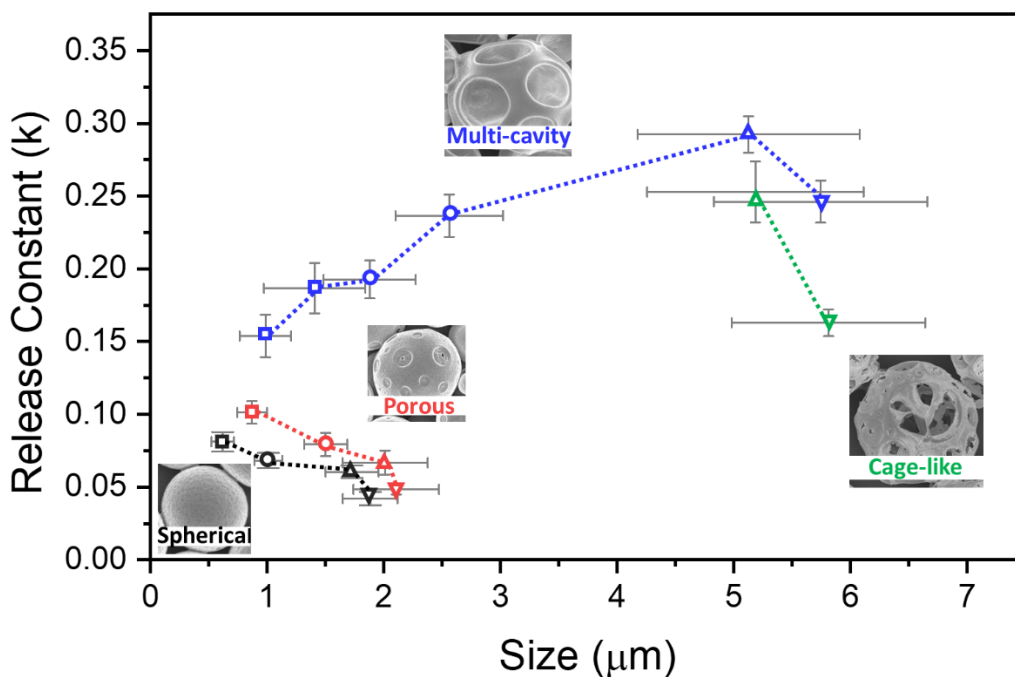


Figure 7: Release rate of RhB for the different formulations of PLGA microparticles. Inset the graph are SEM images of representative particles for that particular microparticle shape. Square, circle, up triangle, and down triangle represent 10%, 5%, 3%, and 1% PVA respectively. Black, red, blue, and green lines represent spherical, porous, multi-cavity, and cage-like microparticles respectively. Data represented as mean \pm standard deviation with a sample size of 3.

541 **Table 1.** Korsmeyer-Peppas model fits of payload released from PLGA microparticles (n=3).

	Geometry	Release Constant (k)	Release exponent (n)	R ²	Release Mechanism
0x PBS					
1% PVA	Spherical	0.042	0.722	0.994	Anomalous Transport
3% PVA	Spherical	0.060	0.663	0.988	Anomalous Transport
5% PVA	Spherical	0.068	0.616	0.994	Anomalous Transport
10% PVA	Spherical	0.081	0.603	0.993	Anomalous Transport
1x PBS					
1% PVA	Porous	0.048	0.679	0.993	Anomalous Transport
3% PVA	Porous	0.067	0.632	0.994	Anomalous Transport
5% PVA	Porous	0.079	0.605	0.983	Anomalous Transport
10% PVA	Porous	0.101	0.575	0.994	Anomalous Transport
10x PBS					
1% PVA	Cage-like	0.163	0.396	0.992	Fickian Diffusion
3% PVA	Cage-like	0.253	0.234	0.952	Fickian Diffusion
5% PVA	Multi-cavity	0.193	0.390	0.976	Fickian Diffusion
10% PVA	Multi-cavity	0.154	0.442	0.957	Anomalous Transport
20x PBS					
1% PVA	Multi-cavity	0.246	0.270	0.959	Fickian Diffusion
3% PVA	Multi-cavity	0.292	0.227	0.966	Fickian Diffusion
5% PVA	Multi-cavity	0.237	0.283	0.953	Fickian Diffusion
10% PVA	Multi-cavity	0.187	0.371	0.933	Fickian Diffusion

542

543

544

545